Accepted Manuscript

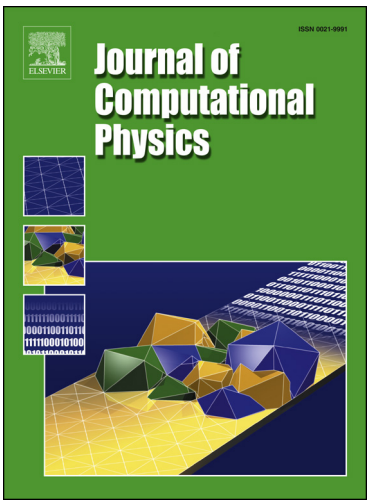

High-order finite-volume modeling of drift waves

M. Dorf, M. Dorr, J. Hittinger, W. Lee, D. Ghosh

PII: S0021-9991(18)30464-9
DOI: https://doi.org/10.1016/j.jcp.2018.07.009
Reference: YJCPH 8134

To appear in: *Journal of Computational Physics*

Received date: 11 July 2017
Revised date: 21 June 2018
Accepted date: 4 July 2018

Please cite this article in press as: M. Dorf et al., High-order finite-volume modeling of drift waves, *J. Comput. Phys.* (2018), https://doi.org/10.1016/j.jcp.2018.07.009

Highlights

- The paper discusses high-order finite-volume numerical modeling of drift waves, which is an ubiquitous phenomenon in magnetized plasmas.
- It is found that standard discretization methods applied to the conservative form of the governing equations can lead to a numerical instability.
- A method to stabilize high-order discretization is proposed and demonstrated to work in numerical simulations performed with the fourth-order finite-volume code COGENT.
- As practical examples, a stable drift-wave solution with adiabatic electrons and the collisionless (universal) drift-wave instability driven by electron kinetic effects are considered.

High-order finite-volume modeling of drift waves

M. Dorf[1], M. Dorr[1], J. Hittinger[1], W. Lee[2], and D. Ghosh[1]

[1]*Lawrence Livermore National Laboratory, Livermore, CA 94550*
[2]*University of California San Diego, La Jolla, CA 92093*

The paper discusses high-order finite-volume numerical modeling of drift waves, which is an ubiquitous phenomenon in magnetized plasmas. It is found that some standard discretization methods applied to the conservative form of the governing equations can lead to a numerical instability. A method to stabilize high-order discretization is proposed and demonstrated to work in numerical simulations performed with the fourth-order finite-volume code COGENT. As practical examples, a stable drift-wave solution with adiabatic electrons and the collisionless (universal) drift-wave instability driven by electron kinetic effects are considered. Application of the present analysis to a broader range of computational fluid dynamics systems is discussed.

I. Introduction.

Drift waves are an ubiquitous phenomenon in a magnetized plasma [1-2]. They are supported by plasma density or temperature gradients, can be destabilized by a variety of physical mechanisms, and play an important role in regulating magnetized plasma transport. It is therefore of significant practical importance to develop advanced numerical methods for the analysis of drift waves and the associated drift-wave turbulence.

The governing equations for magnetized plasma dynamics, including the effects of drift-waves, can be written in a conservative form (i.e., expressed as a divergence of a flux function), thereby motivating the use of finite-volume methods, which satisfy a discrete from of the divergence theorem [3-4]. Finite-volume methods have traditionally been applied in first or second order, but the evolution of computer architectures encourages the use of higher-order [5]. Recently, Colella *et al* [6] developed a useful framework for constructing finite-volume methods in mapped coordinates of any order of accuracy. The method proposed in Ref. [6] was then extended to the case of a mapped multiblock grid system [7], where the entire grid structure is represented by a union of grid blocks with a smooth function defined on each block to map the physical coordinate system onto a logically-rectangular (computational) grid and with high-order interpolation methods used for intra-block communication. That development enabled the application of high-order finite-volume methods to complex-geometry systems, such as the edge of a divertor tokamak. In particular, the numerical algorithms developed in Ref. [6-7] were employed in the high-order (4^{th}-order) continuum gyrokinetic code COGENT to study magnetized plasma transport in the edge of a tokamak [8-12].

While the COGENT code was successfully applied to a variety of magnetized plasma transport problems [8-11], an unexpected numerical instability has been observed for the case of a drift-wave problem, even when considered in the simplest case of a slab (Cartesian) geometry. In this paper, we discuss the underlying mechanisms for such instability and propose a stabilization method. It is found that the conservative form of the governing equations for magnetized plasma dynamics includes $E \times B$ advection terms that can individually drive strongly-unstable modes, but analytically should cancel each other. This important cancellation does not necessarily occur numerically for an arbitrary high-order discretization scheme, thus leading to a numerical instability. However, a stable discretization, i.e., that provides discrete cancelation of the required

terms, is identified and demonstrated to work in COGENT simulations. We note that while the discovered numerical instability appears in some high-order finite-volume discretization schemes, other numerical schemes such as finite-difference, spectral, and finite-element (with C^1 continuous elements) appear to be stable in this respect.

The paper is organized as follows: In Sec. II, a simple hydrodynamic (fluid) drift-wave model is considered, for which the mechanism of the numerical instability is elucidated and an approach to a stable discretization is presented. The analysis is extended to a kinetic description in Sec. III, and the stabilizing method is demonstrated to work in 4th-order COGENT simulations. As practical examples, we consider a stable drift-wave solution with adiabatic electrons [Sec. III (a)] and the collisionless (universal) drift-wave instability driven by electron kinetic effects [Sec. III (b)]. The conclusions of the present work and its relevance to a wider range of fluid dynamics systems are discussed in Sec. IV.

II. Model equations

A simple linear model that describes the long-wavelength limit of electrostatic drift-waves in a magnetized plasma for the case of cold ions and adiabatic electrons is given by the following set of equations:

$$\frac{\partial}{\partial t}\delta n + \nabla \cdot (n_0 \boldsymbol{V}) = 0, \tag{1}$$

$$\boldsymbol{V} = c\,\frac{-\boldsymbol{\nabla}\phi \times \mathbf{B}}{B^2}, \tag{2}$$

$$\frac{e\phi}{T_e} = \frac{\delta n}{n_0}. \tag{3}$$

Here, δn and ϕ are perturbations of plasma density and electrostatic potential, respectively, $n_0 = n_0(x)$ is the background plasma density, $\boldsymbol{V}$ is the ion gyrocenter velocity, $\mathbf{B} = B\hat{\mathbf{z}}$ is the magnetic field, e and c denotes the elementary charge and the speed of light in vacuum, and T_e is the electron temperature, which is assumed to be uniform along magnetic field lines. Considering, for simplicity, $B = const$ and $T_e = const$, we obtain the following equation for the electrostatic potential perturbations:

$$\frac{\partial}{\partial t}\left(n_0 \frac{e\phi}{T_e}\right) = \frac{\partial}{\partial x}\left(-\frac{c}{B} n_0 \frac{\partial \phi}{\partial y}\right) + \frac{\partial}{\partial y}\left(\frac{c}{B} n_0 \frac{\partial \phi}{\partial x}\right). \tag{4}$$

Equation (4) represent the governing equation for the drift-wave dynamics written in the conservative form, i.e., expressed as a divergence of a flux function. Expanding the spatial derivatives of the *flux* quantities we obtain

$$\frac{\partial \phi}{\partial t} = -V_{dr}\frac{\partial \phi}{\partial y} + \frac{T_e c}{eB}\left[-\frac{\partial}{\partial x}\left(\frac{\partial \phi}{\partial y}\right) + \frac{\partial}{\partial y}\left(\frac{\partial \phi}{\partial x}\right)\right], \tag{5}$$

where $V_{dr} = T_e c L_n^{-1}/eB$ is the so-called drift velocity and $L_n^{-1} = n_0^{-1}(dn_0/dx)$. Noticing that the last two terms in Eq. (5) inside the square brackets exactly cancel each other for a smooth

function $\phi(x,y,t)$, we obtain a simple advection equation for the drift-waves propagating in the y–direction.

(a) Stability issues of a general high-order finite-volume discretization

While Eq. (4) [or, Eq. (5)] has only stable solutions in the continuum space, it is found that an arbitrary numerical discretization of this equation can yield numerically unstable solutions. This fact can be elucidated as follows. Although, the last two terms in Eq. (5) exactly cancel each other, each of them independently can drive a strong instability with the growth rate, $\gamma = (T_e c/eB)k_x k_y$. Here, k_x and k_y are the wave vectors in the *x* and *y* directions, respectively. Therefore, if a discrete cancellation of those terms is not enforced, a numerical instability can potentially develop. In what follows, we support this heuristic argument by directly analyzing stability properties of the standard 4th-order central-difference finite-volume discretization proposed in Ref. [6]. To simplify the problem, we consider the case of a uniform background density $n_0 = const$, which is still prone to the numerical instability as evident from Eq. (5). Introducing the normalization parameter $D_B = cT_e/(eB)$ and the flux function $\mathbf{\Gamma} = [\hat{\boldsymbol{z}} \times \boldsymbol{\nabla}\phi]$, Eq. (4) takes the following form

$$\frac{\partial D_B^{-1}\phi}{\partial t} = \frac{\partial \Gamma_x}{\partial x} + \frac{\partial \Gamma_y}{\partial y}. \tag{6}$$

The numerical discretization of Eq. (6) is obtained as follows [6]. The spatial domain (x,y) is discretized as a union of rectangular control volumes

$$V_{\mathbf{i}} = \left[x_{i_x} - \frac{h}{2}, x_{i_x} + \frac{h}{2}\right] \times \left[y_{i_y} - \frac{h}{2}, y_{i_y} + \frac{h}{2}\right], \tag{7}$$

where the multi-index $\mathbf{i} = (i_x, i_y)$ is identified with the location of the control volume center, and an equal grid spacing h is assumed in both directions. Integrating Eq. (6) over a control volume, it follows that

$$\frac{\partial}{\partial t}\langle\langle\phi\rangle\rangle_{\mathbf{i}} = \frac{D_B}{h}\sum_{d=x,y}\left(\langle\Gamma_d\rangle_{\mathbf{i}+\frac{1}{2}\mathbf{e}^d} - \langle\Gamma_d\rangle_{\mathbf{i}-\frac{1}{2}\mathbf{e}^d}\right). \tag{8}$$

Here, $\mathbf{e}^d$ is the unit vector in the direction d, and the operators $\langle\langle\cdot\rangle\rangle_{\mathbf{i}}$ and $\langle\cdot\rangle_{\mathbf{i}\pm\frac{1}{2}\mathbf{e}^d}$ denote an average over the cell centered at $\mathbf{i}$ and averages over the faces centered at $\mathbf{i} \pm \frac{1}{2}\mathbf{e}^d$, respectively. Face-averaged fluxes can be expressed via face-centered flux values to fourth-order accuracy by [6]

$$\langle\Gamma_d\rangle_{\mathbf{i}+\frac{1}{2}\mathbf{e}^d} = \Gamma_{d,\mathbf{i}+\frac{1}{2}\mathbf{e}^d} + \frac{1}{24}\sum_{\substack{d'=x,y \\ d'\neq d}}\left(\Gamma_{d,\mathbf{i}+\frac{1}{2}\mathbf{e}^d+\mathbf{e}^{d'}} + \Gamma_{d,\mathbf{i}+\frac{1}{2}\mathbf{e}^d-\mathbf{e}^{d'}} - 2\Gamma_{d,\mathbf{i}+\frac{1}{2}\mathbf{e}^d}\right) + O(h^4). \tag{9}$$

The discrete fluxes in the right-hand-side of Eq. (9) are related to the gradient of the potential by $\mathbf{\Gamma}_{\mathbf{i}+\frac{1}{2}\mathbf{e}^d} = \left[\hat{\boldsymbol{z}} \times (\boldsymbol{\nabla}\phi)_{\mathbf{i}+\frac{1}{2}\mathbf{e}^d}\right]$ and can be evaluated by making use of the approximation

$$(\nabla_{d'}\phi)_{\mathbf{i}+\frac{1}{2}\mathbf{e}^d} = \frac{1}{h}\left(-\frac{1}{12}\phi_{\mathbf{i}+\frac{1}{2}\mathbf{e}^d+2\mathbf{e}^{d'}} + \frac{2}{3}\phi_{\mathbf{i}+\frac{1}{2}\mathbf{e}^d+\mathbf{e}^{d'}} - \frac{2}{3}\phi_{\mathbf{i}+\frac{1}{2}\mathbf{e}^d-\mathbf{e}^{d'}} + \frac{1}{12}\phi_{\mathbf{i}+\frac{1}{2}\mathbf{e}^d-2\mathbf{e}^{d'}}\right) + O\left(h^4\right). \tag{10}$$

The face-centered potential values in Eq. (10) are related to the corresponding cell-centered values by

$$\phi_{\mathbf{i}+\frac{1}{2}\mathbf{e}^d} = \frac{1}{16}\left(9\phi_{\mathbf{i}+\mathbf{e}^d} + 9\phi_{\mathbf{i}} - \phi_{\mathbf{i}+2\mathbf{e}^d} - \phi_{\mathbf{i}-\mathbf{e}^d}\right) + O\left(h^4\right), \tag{11}$$

and the final step to close the discretization system is to express the cell-centered values in terms of the cell-averages, $\langle\langle\phi\rangle\rangle_{\mathbf{i}}$,

$$\phi_{\mathbf{i}} = \langle\langle\phi\rangle\rangle_{\mathbf{i}} - \frac{1}{24}\sum_{d=x,y}\left(\langle\langle\phi\rangle\rangle_{\mathbf{i}+\mathbf{e}^d} + \langle\langle\phi\rangle\rangle_{\mathbf{i}-\mathbf{e}^d} - 2\langle\langle\phi\rangle\rangle_{\mathbf{i}}\right) + O\left(h^4\right). \tag{12}$$

Equations (8)-(12) represent a fourth-order central-differencing finite-volume discretization of Eq. (6).

We now analyze the linear stability properties of the discretization in Eq. (8)-(12) by assuming a spatially discrete solution in the form of

$$\langle\langle\phi\rangle\rangle_{\mathbf{i}} = \frac{1}{24}\mathrm{Re}\{\exp(\gamma t + Ik_x i_x + Ik_y i_y)\}. \tag{13}$$

Here, the discrete wave-vectors $k_{x,y}$ can take the values of $k_{x,y} = 2\pi h^{-1} n_{x,y}/N_{x,y}$, where $N_{x,y}$ is the number of grid points in the x and y directions, respectively, and $n_{x,y} = 0, \ldots, N_{x,y} - 1$. Combining Eq. (13) with Eq. (6) by making use of the symbolic computation package Mathematica [13], we obtain

$$\begin{aligned}\frac{\gamma}{D_B} = -\frac{\sin(hk_x)\sin(hk_y)}{13824h^2}\big[&962\cos(hk_x) - 316\cos(2hk_x) + 10\cos(3hk_x)\\ &+ \cos(hk_x - 3hk_y) - 38\cos(hk_x - 2hk_y) + 38\cos(2hk_x - hk_y)\\ &- \cos(3hk_x - hk_y) - 962\cos(hk_y) + 316\cos(2hk_y)\\ &- 10\cos(3hk_y) + 38\cos(2hk_x + hk_y) - \cos(3hk_x + hk_y)\\ &- 38\cos(hk_x + 2hk_y) + \cos(hk_x + 3hk_y)\big].\end{aligned} \tag{14}$$

In the long-wavelength limit, $hk_{x,y} \ll 1$, Eq. (14) gives

$$\frac{\gamma}{D_B} = -\frac{k_x k_y\left(k_y^4 - k_x^4\right)}{144}h^4 + O(h^5), \tag{15}$$

which is consistent with a fourth-order discretization of the right-hand-side of Eq. (6) corresponding to a zero function in the continuum space. However, at high wavelengths, $hk_{x,y}\sim 1$, Eq. (14) predicts unstable solutions with $\gamma\sim D_B h^{-2}$, in accordance with the heuristic arguments presented earlier. For instance, taking $hk_x = \pi/2$ and $hk_y = \pi/4$, we obtain $\gamma = 0.021 D_B h^{-2}$.

We note again that the numerical instability appears when a discretization scheme does not annihilate the right-hand-side of Eq. (8). It is straightforward to show that a 2nd-order finite-volume central-difference scheme yields discrete cancellation of the unstable drive terms and, therefore, is numerically stable. The same is true for an arbitrary-order finite-differencing scheme including centered and/or forward/backward stencils, spectral scheme, and finite element scheme with C^1 elements. However, an arbitrary high-order (e.g., 4th-order) central-difference finite-volume discretization [e.g., given in Eqs. (8) – (12)], cannot guarantee numerical stability of the drift-wave problem.

(b) A method to stabilize a high-order finite-volume discretization

A stable discretization should annihilate the right-hand-side of Eq. (8), which can be achieved if, instead of using Eq. (9), we directly compute the face-averaged fluxes in Eq. (8) as

$$\langle \Gamma_x \rangle_{\mathbf{i}\pm\frac{1}{2}\mathbf{e}^x} = -\phi_{d,\mathbf{i}\pm\frac{1}{2}\mathbf{e}^x+\frac{1}{2}\mathbf{e}^y} + \phi_{d,\mathbf{i}\pm\frac{1}{2}\mathbf{e}^x-\frac{1}{2}\mathbf{e}^y}\,, \tag{16}$$

$$\langle \Gamma_y \rangle_{\mathbf{i}\pm\frac{1}{2}\mathbf{e}^y} = \phi_{d,\mathbf{i}\pm\frac{1}{2}\mathbf{e}^y+\frac{1}{2}\mathbf{e}^x} - \phi_{d,\mathbf{i}\pm\frac{1}{2}\mathbf{e}^y-\frac{1}{2}\mathbf{e}^x}\,. \tag{17}$$

Note that Eqs. (16) – (17) are exact formulas for the flux quadrature. The cell-corner quantities in the right-hand-side of Eq. (16)-(17) can now be expressed via cell-averaged values $\langle\langle\phi\rangle\rangle_{\mathbf{i}}$ by making use of an arbitrary high-order approximation (e.g., bicubic interpolation), while maintaining the overall stability of a discretization scheme.

The numerical stability analysis in Eq. (6) – (17) is performed for the case of a uniform background density, which does not formally support the drift waves. We now demonstrate that the method to compute flux quadrature in Eq. (16) – (17) provides stability of a high-order finite volume discretization applied to the original system [in Eq. (4)], where the background density can vary in the x-direction and where drift waves can be observed. Integrating Eq. (4) over a control volume, we obtain

$$\frac{\partial}{\partial t}\langle\langle n_0\phi\rangle\rangle_{\mathbf{i}} = \frac{D_B}{h}\sum_{d=x,y}\left(\langle n_0\Gamma_d\rangle_{\mathbf{i}+\frac{1}{2}\mathbf{e}^d} - \langle n_0\Gamma_d\rangle_{\mathbf{i}-\frac{1}{2}\mathbf{e}^d}\right). \tag{18}$$

The face-averaged fluxes in the right-hand-side of Eq. (18) can be written in terms of the face-averages $\langle n_0\rangle_{\mathbf{i}\pm\frac{1}{2}\mathbf{e}^d}$ and $\langle \Gamma_y\rangle_{\mathbf{i}\pm\frac{1}{2}\mathbf{e}^d}$ and the pointwise values of the gradients of n_0 and Γ_y at the face centers as

$$\langle n_0\Gamma_d\rangle_{\mathbf{i}\pm\frac{1}{2}\mathbf{e}^d} = \langle n_0\rangle_{\mathbf{i}\pm\frac{1}{2}\mathbf{e}^d}\langle\Gamma_y\rangle_{\mathbf{i}\pm\frac{1}{2}\mathbf{e}^d} + \frac{h^2}{12}\sum_{\substack{d'=x,y\\ d'\neq d}}\left(\frac{\partial n_0}{\partial\xi_{d'}}\frac{\partial\Gamma_d}{\partial\xi_{d'}}\right)_{\mathbf{i}\pm\frac{1}{2}\mathbf{e}^d} + O(h^4), \tag{19}$$

where $\xi_x = x$ and $\xi_y = y$. Combining Eq. (19) with Eq. (18) and performing some straightforward algebra, we obtain

$$\begin{aligned}\frac{\partial}{\partial t}\langle\langle n_0\phi\rangle\rangle_{\mathbf{i}} = {}& \frac{D_B}{h}\langle\Gamma_x\rangle_{\mathbf{i}+\frac{1}{2}\mathbf{e}^x}\left((n_0)_{\mathbf{i}+\frac{1}{2}\mathbf{e}^x} - \langle n_0\rangle_{\mathbf{i}}\right) + \frac{D_B}{h}\langle\Gamma_x\rangle_{\mathbf{i}-\frac{1}{2}\mathbf{e}^x}\left(\langle n_0\rangle_{\mathbf{i}} - (n_0)_{\mathbf{i}-\frac{1}{2}\mathbf{e}^x}\right)\\ &+\frac{D_B}{h}\langle n_0\rangle_{\mathbf{i}}\sum_{d=x,y}\left(\langle\Gamma_d\rangle_{\mathbf{i}+\frac{1}{2}\mathbf{e}^d} - \langle\Gamma_d\rangle_{\mathbf{i}-\frac{1}{2}\mathbf{e}^d}\right)\\ &+D_B h\left(\frac{\partial n_0}{\partial x}\right)_{\mathbf{i}}\left[\left(\frac{\partial\Gamma_y}{\partial x}\right)_{\mathbf{i}+\frac{1}{2}\mathbf{e}^y} - \left(\frac{\partial\Gamma_y}{\partial x}\right)_{\mathbf{i}-\frac{1}{2}\mathbf{e}^y}\right] + O(h^4),\end{aligned} \tag{20}$$

where it is used that $\partial n_0/\partial y = 0$ and $\langle n_0\rangle_{\mathbf{i}}$ denotes the density average over the faces centered at i_x. The terms on the first line in Eq. (20) describe a drift-wave oscillation to a low-order (2nd-order) accuracy; the terms on the second line correspond to the right-hand-side of Eq. (8) and exactly cancel each other provided the discretization in Eqs. (16)-(17) is used; and finally, the terms on the third line correspond to higher-order corrections. The higher-order corrections represent

discretization of the term $\propto h^2\,\partial^3\phi/\partial y\partial x^2$ and therefore can only yield a correction to the drift-wave frequency and do not drive instability.

Finally, we note that the simple long-wavelength $k_\perp\rho_s$<<1 model for the drift waves in Eqs. (1)-(3) does not include small corrections of order $O(k_\perp^2\rho_s^2)$ related to the ion polarization density. Here, $k_\perp$is magnitude of the perturbation wave-vector in the plane perpendicular to the magnetic field, $\rho_s = (m_i c/eB)\sqrt{2T_e/m_i}$, and m_i is the ion mass. If such corrections are retained, Eq. (3) takes the following form

$$\frac{m_i c^2}{B^2}\boldsymbol{\nabla}_\perp(n_0\boldsymbol{\nabla}_\perp\phi) = \frac{e^2\phi}{T_e}n_0 - e\delta n, \tag{21}$$

which corresponds to

$$\frac{e\phi_{\mathbf{k}}}{T_e} = \frac{\delta n_{\mathbf{k}}}{n_0(1 + k_\perp^2\rho_s^2/2)}, \tag{22}$$

in the Fourier space assuming that $k_\perp L_n \gg 1$. It is now easy to show that each of the "destabilizing" terms discussed in Sec. II (a) can potentially drive the instability with the growth rate of $\gamma\sim(T_e c/eB)k_x k_y(1 + k_\perp^2\rho_s^2)^{-1}$. Repeating the discretization analysis in Eqs. (6)-(16), it is straightforward to demonstrate that in the limit of $h \to 0$, the numerical instability growth rate does not become infinite, but is bounded by $\gamma\sim D_B\rho_s^{-2}$.

III. COGENT implementation

Here, the analysis in Sec. II is extended to a kinetic description of drift waves, and the method to stabilize high-order finite-volume discretization [in Eqs. (16) – (17)] is demonstrated to work in numerical simulations performed with the fourth-order kinetic code COGENT. As practical examples, we consider a stable drift-wave solution with adiabatic electrons [Sec. III (a)] and the collisionless (universal) drift-wave instability driven by electron kinetic effects [Sec. III (b)].

The COGENT code describes magnetized plasma dynamics in arbitrary magnetic geometries, including a single-null divertor geometry, by solving a system of gyrokinetic equations for multiple species coupled to the long-wave limit of the gyro-Poisson equations [9-11, 14]. For illustrative purposes, here we consider a singly-charged collisionless plasma immersed in a uniform magnetic field $\mathbf{B} = B_y\mathbf{e}^y + B_z\mathbf{e}^z = const$, and assume that there are no variations in the z-direction, i.e., $\partial/\partial z = 0$. For this case, the governing equations for the gyro-averaged distribution function $f_\alpha(x, y, v_\parallel, \mu)$ are given in the conservative form by

$$\frac{\partial f_\alpha}{\partial t} + \sum_{d=x,y,v_\parallel,\mu}\frac{\partial}{\partial\xi_d}(V_d f_\alpha) = 0, \tag{23}$$

$$\frac{m_i c^2}{B^2}\boldsymbol{\nabla}_\perp(n\boldsymbol{\nabla}_\perp\phi) = -\sum_\alpha q_\alpha\int\left(\frac{2\pi B}{m_\alpha}\right)f_\alpha dv_\parallel d\mu\,, \tag{24}$$

where the long-wavelength limit $k_\perp\rho_i$<<1 is assumed, $\boldsymbol{\nabla}_\perp$ is the gradient operator in the plane perpendicular to the magnetic field, and the 4D phase-space velocity V_d is specified by

$$V_x = -\frac{cB_z}{B^2}\frac{\partial \phi}{\partial y}, \tag{25}$$

$$V_y = -\frac{B_y}{B}v_\parallel + c\frac{B_z}{B^2}\frac{\partial \phi}{\partial x}, \tag{26}$$

$$V_{v_\parallel} = -\frac{q_\alpha}{m_\alpha}\frac{B_y}{B}\frac{\partial \phi}{\partial y}, \tag{27}$$

$$V_\mu = 0. \tag{28}$$

Here, B is the magnetic field magnitude, q_α and m_α are the species charge and mass, respectively, and the subscript α designates the electron (e) or singly-charged ion (i) species. The Vlasov equation [i.e., Eq. (23)] is discretized in the usual way by integrating over a 4D control volume,

$$\frac{\partial}{\partial t}\langle\langle f_\alpha\rangle\rangle_{\mathbf{i}} = \frac{1}{h_d}\sum_d \left(\langle V_d f_\alpha\rangle_{\mathbf{i}+\frac{1}{2}\mathbf{e}^d} - \langle V_d f_\alpha\rangle_{\mathbf{i}-\frac{1}{2}\mathbf{e}^d}\right) \tag{29}$$

and employing the 4-th order formula for the flux face-averages [6] to obtain

$$\langle V_d f_\alpha\rangle_{\mathbf{i}\pm\frac{1}{2}\mathbf{e}^d} = \langle V_d\rangle_{\mathbf{i}\pm\frac{1}{2}\mathbf{e}^d}\langle f_\alpha\rangle_{\mathbf{i}\pm\frac{1}{2}\mathbf{e}^d} + \sum_{d'\neq d}\frac{h_{d'}^2}{12}\left(\frac{\partial\langle V_d\rangle}{\partial \xi_{d'}}\right)_{\mathbf{i}\pm\frac{1}{2}\mathbf{e}^d}\left(\frac{\partial\langle f_\alpha\rangle}{\partial \xi_{d'}}\right)_{\mathbf{i}\pm\frac{1}{2}\mathbf{e}^d} + O\left(h^4\right), \tag{30}$$

where a second-order accurate difference approximation to the $\partial/\partial\xi$ derivatives is used. Here, $h_d \propto h$ denotes a grid spacing in the direction d. We note that $\langle V_x\rangle_{\mathbf{i}\pm\frac{1}{2}\mathbf{e}^d} = (cB_z/B^2)\langle \Gamma_x\rangle_{\mathbf{i}\pm\frac{1}{2}\mathbf{e}^d}$ and $\langle V_y\rangle_{\mathbf{i}\pm\frac{1}{2}\mathbf{e}^d} = -\left(B_y/B\right)\langle v_\parallel\rangle_{\mathbf{i}\pm\frac{1}{2}\mathbf{e}^d} + (cB_z/B^2)\langle \Gamma_y\rangle_{\mathbf{i}\pm\frac{1}{2}\mathbf{e}^d}$, where $\boldsymbol{\Gamma} = [\hat{\boldsymbol{z}}\times\boldsymbol{\nabla}\phi]$ (as in Sec. II). Therefore, in order to obtain a stable discretization, we compute the face averages $\langle V_d\rangle_{\mathbf{i}\pm\frac{1}{2}\mathbf{e}^d}$ by making use of Eqs. (16) and (17). Other details on the COGENT implementation of gyro-kinetic [i.e., Eq. (23)] and gyro-Poisson [i.e., Eq. (24)] equations can be found in Refs. [8] and [12]. In particular, various options, including high-order upwind and WENO methods, are available to compute the distribution function face-averages $\langle f_\alpha\rangle_{\mathbf{i}\pm\frac{1}{2}\mathbf{e}^d}$. For the simulations presented in this section, the limited 4$^{\text{th}}$-order WENO-like scheme developed in Ref. [15] is used. For the time discretization, an explicit 4$^{\text{th}}$-order Runge-Kutta scheme is employed.

(a) Stable drift-wave solution with adiabatic electrons

As a simple illustrative example, here we consider the case of a linearized adiabatic electron response, for which we adopt Eq. (3), i.e., $(n_e - n_0)/n_0 = e\phi/T_e$. Here, $n_e$and n_0 are the electron and background plasma density, respectively, and $T_e = const$ is assumed. Furthermore, we neglect the polarization ion density term, i.e., the left-hand-side of Eq. (24), and take $B_y = 0$. Under these assumptions a small-signal linear solution of Eqs. (23)-(24) is equivalent to a solution of Eq. (4).

We consider a rectangular computational domain with $L_x = L_y = L$ and periodic boundary conditions in the both spatial directions. The initial ion distribution function is given by a Maxwellian distribution, $F_{0,i} = n_0(m_i/2\pi T_i)^{3/2}\exp\left(-m_i v_\parallel^2/2T_i - \mu B/T_i\right)$, with a uniform temperature T_i, and a density distribution given by $n_0 = \bar{n}(1+\sin^2(\pi x/L))(1+\epsilon\cos(4\pi y/L))$, where the perturbation amplitude corresponds to $\epsilon = 10^{-6}$, and the domain extents of the velocity space, $-v_{\parallel,max} < v_\parallel < v_{\parallel,max}$, and $0 < \mu < \mu_{max}$ are $m_i v_{\parallel,max}^2/2T_i = 12.25$ and $\mu_{max}B/T_i = 12$, respectively. The linear analytic solution is given by

$$\frac{e\phi_{AN}(t,x,y)}{T_e} = \epsilon\cos\left\{\frac{4\pi}{L}[y - V_{dr}(x)t]\right\}, \tag{31}$$

where the drift velocity is specified by $V_{dr} = (T_e c/eB)(\pi/L)\sin(2\pi x/L)\,(1+\sin^2(\pi x/L))^{-1}$. The numerical COGENT solution, ϕ^{COG}, is compared against the analytic solution in Eq. (31) at the time instant, t, roughly corresponding to a half-period of a drift wave oscillation $(T_e c/eB)(4\pi^2/L^2)t = 3.36$. The results for the maximum numerical error computed as

$$Er = \epsilon^{-1}\frac{e}{T_e}\max_{\mathbf{i}}\left|\phi_{AN}(t,x_\mathbf{i},y_\mathbf{i}) - \phi_\mathbf{i}^{COG}(t)\right|, \tag{32}$$

are shown in Fig. 1. Here, $\phi_\mathbf{i}^{COG}$ is the cell-centered numerical solution. For comparison purposes, the results from second-order accurate COGENT calculations are presented as well.

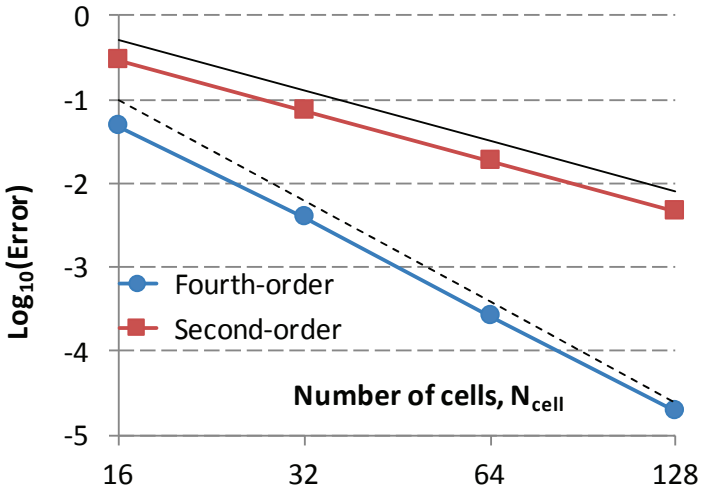

Fig. 1. COGENT convergence studies for the case of stable drift-wave oscillations with the adiabatic electron response. The number of cells per phase-space direction is $(N_x, N_y, N_{v_\parallel}, N_\mu) = (N_{\text{cell}}, N_{\text{cell}}, N_{\text{cell}}/2, 3N_{\text{cell}}/8)$, and the time step, Δt, corresponds to $(T_e c/eB)(4\pi^2/L^2)\Delta t = 10.75/N_{\text{cell}}$. The results of the COGENT simulations are shown with the blue circles (4^{th}-order) and red squares (2^{nd}-order). The dashed and solid lines illustrate the fourth and second order convergence rate, respectively.

(b) Unstable drift-wave solution with kinetic electrons

We now adopt a fully-kinetic electron response and retain the ion polarization-density term, i.e., we consider the full set of Eqs. (23)-(24). In Sec. 3(a), it is demonstrated that the adiabatic

electron response corresponding to $\omega/k_\parallel \ll V_{T,e}$ can only support stable drift-wave oscillations [see Eq. (31)]. Here, we show that retaining the kinetic electron effects of order $O\left(\omega/V_{T,e}k_\parallel\right)$ yields the so-called universal drift-wave instability [1-2]. The instability is driven by the Landau damping effect, which acts as a kinetic "resistive-drive" mechanism, and therefore the maximum growth rate occurs at $\omega \sim V_{T,e}k_\parallel$.

For illustrative purposes, we consider the case of a uniform background temperature for both ion and electron species. Introducing the complex perturbation amplitudes, $\tilde{f}_\alpha$ and $\tilde{\phi}$, such that $f_\alpha = F_{0,\alpha} + Re\left\{\tilde{f}_\alpha(x, v_\parallel)\exp\left(-I\omega t + Ik_y y\right)\right\}$ and $\phi = Re\left\{\tilde{\phi}(x)\exp\left(-I\omega t + Ik_y y\right)\right\}$, and linearizing Eq. (23), we obtain

$$\tilde{f}_\alpha = \frac{\frac{cB_z}{B^2}k_y\tilde{\phi}\,L_n^{-1}F_{0,\alpha} - \frac{q_\alpha}{T_\alpha}k_y\frac{B_y}{B}\tilde{\phi}v_\parallel F_{0,\alpha}}{-\omega + \left(B_y/B\right)k_y v_\parallel}, \tag{33}$$

where $F_{0,\alpha}$ is the unperturbed Maxwellian background with a uniform temperature T_α and a varying density profile $n_0(x)$. Integrating Eq. (33) over the velocity space and performing some straightforward algebra gives

$$\int \tilde{f}_\alpha d^3v = -\frac{q_\alpha n_0\tilde{\phi}}{T_\alpha}\left[1 - (\omega - \omega_\alpha^*)\int d^3v\frac{n_0^{-1}F_{0,\alpha}}{\omega - \left(B_y/B\right)k_y v_\parallel}\right], \tag{34}$$

where we introduced the drift frequency

$$\omega_\alpha^* = \frac{cT_\alpha L_n^{-1}}{Bq_\alpha}k_y\frac{B_z}{B}\ . \tag{35}$$

Combining Eq. (34) and Eq. (24), we obtain an eigenvalue equation for the complex potential amplitude $\tilde{\phi}(x)$

$$\frac{m_i c^2}{B^2}\left(\frac{B_z^2}{B^2}k_y^2 - \frac{\partial^2}{\partial x^2} - L_n^{-1}\frac{\partial}{\partial x}\right)\tilde{\phi}(x) = -\frac{q_\alpha^2\tilde{\phi}}{T_\alpha}\left[1 + \frac{(\omega - \omega_\alpha^*)}{k_\parallel v_{T,\alpha}}\int_{-\infty}^{+\infty}dt\frac{\pi^{-1/2}\exp(-t^2)}{t - \frac{\omega}{k_\parallel v_{T,\alpha}}}\right], \tag{36}$$

where $v_{T,\alpha} = \sqrt{2T_\alpha/m_\alpha}$ and $k_\parallel = \left(B_y/B\right)k_y$. In order to make analytic progress, we consider a zero Dirichlet boundary condition for the potential perturbations in the x-direction and a periodic boundary condition in the y-direction. Furthermore, we take $L_n^{-1} = n_0^{-1}(dn_0/dx) = const$ and assume $L_n k_\perp \gg 1$, such that the term $L_n^{-1}\partial/\partial x$ in the left-hand-side of Eq. (36) can be neglected. Under these assumptions, a solution for the complex amplitude of a potential perturbation is given by $\tilde{\phi} = \exp\left(-I\omega t + Ik_x x + Ik_y y\right)$, where $k_x = \pi n_x/L_x$, $k_y = 2\pi n_y/L_y$, $n_{x,y}$ is the mode number in the x and y directions, and the frequency, ω, is found from Eq. (36), which now represents an algebraic equation. In the limit of $v_{T,i} \ll \omega/k_\parallel \ll v_{T,e}$ corresponding to the cold ions and nearly-adiabatic electrons, it is straightforward to obtain [1-2]

$$1 - \frac{\omega_e^*}{\omega} + \frac{1}{2}\rho_s^2 k_\perp^2 = I\sqrt{\pi}\frac{\omega_e^* - \omega}{\left|k_\parallel\right|v_{T,e}}, \tag{37}$$

where $k_\perp^2 = (B_z/B)^2 k_y^2 + k_x^2$. Assuming $\rho_s k_\perp \ll 1$, we obtain to a leading order that $\mathrm{Re}(\omega) \approx \omega_e^*$ and $Im(\omega) \approx \left(\sqrt{\pi}/2\right)(\rho_s^2 k_\perp^2)\,(\omega_e^*)^2/\left(\left|k_\parallel\right|v_{T,e}\right)$.

The collisionless drift-wave instability is modeled with the COGENT code. For these simulations, we consider a rectangular simulation domain with $L_x = L_y = L$. The initial species distributions are given by Maxwellian distribution functions, $F_{0,\alpha} = n_\alpha^0 \, (m_\alpha/2\pi T_\alpha)^{3/2} \exp\left(-m_\alpha v_\parallel^2/2T_\alpha - \mu B/T_\alpha\right)$, with uniform temperature distributions $T_i = T_e = T_0$ and density distributions given by $n_i^0 = n_e^0 = \bar{n}\exp(-x/4L) + \epsilon\bar{n}\cos(2\pi y/L)\sin(\pi x/L)$, where the perturbation amplitude corresponds to $\epsilon = 10^{-5}$, and the domain extents of the velocity space, $-v_{\parallel,max} < v_\parallel < v_{\parallel,max}$, and $0 < \mu < \mu_{max}$ are $m_\alpha v_{\parallel,max}^2/2T_0 = 8$ and $\mu_{max}B/T_0 = 7.5$, respectively. Note that the background density profile has a constant logarithmic spatial derivative $L_n = -4L$. Other numerical parameters correspond to $B_y = B_z/300$, $m_e = m_i/200$, $\rho_i/L = 0.17$. A periodic boundary condition is used for both potential and distribution function in the y – direction. In the x–direction, a zero Dirichlet boundary condition is imposed on the potential. This inhibits particle flows across the x–boundaries and therefore inflow boundary conditions for the distribution function at the x–boundaries are not required. The analysis of the linear dispersion equation in Eq. (36) for the parameters of COGENT simulations show that the seeded perturbation with $n_x = 1/2$ and $n_y = 1$ has the maximal growth rate. Note that such perturbation corresponds to $k_\perp\rho_i \approx 1$, and therefore neither simulations nor Eq. (36) can accurately predict its physical behavior. However, being the fastest growing mode it is convenient to consider such a perturbation for illustrative purposes.

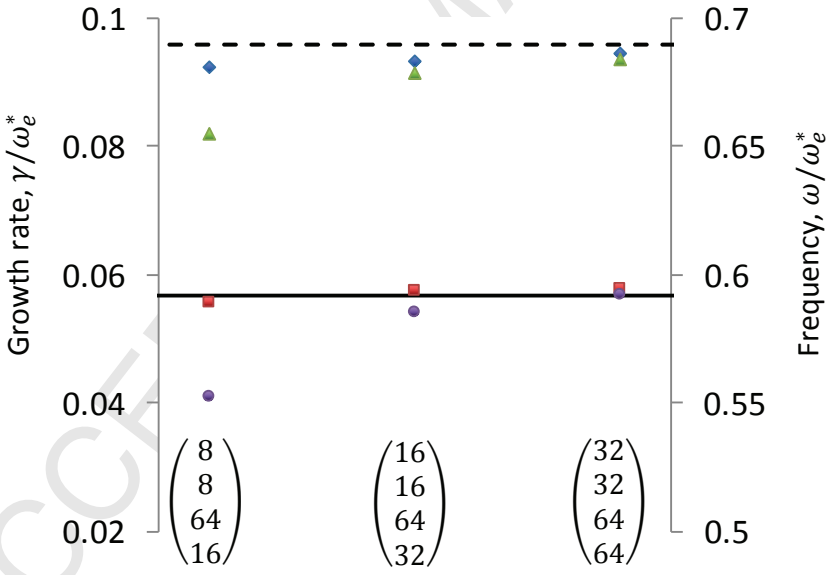

Fig. 2. COGENT convergence studies for the case of the collisionless (universal) drift-wave instability. The fourth-order results for the growth rate (blue diamonds) and real frequency (red squares) are compared with the corresponding second-order results (shown with green triangles and purple circles). The numerical solution to Eq. (36) (neglecting the term $L_n^{-1}\partial/\partial x$) is illustrated with the dashed and solid lines for the growth rate and real frequency, respectively. The number of cells in each direction is shown under the data sets in the order (top-to-bottom) of x, y, $v_\parallel$, and μ. Due to kinetic nature of the instability, maintaining high resolution in the parallel velocity space for this convergence study is found to be important in order to obtain the fastest-growing mode number consistent with the analytical predictions. The time step in simulations corresponds to $\omega_e^*\Delta t = 0.2 \times (8/N_{cell})$, where N_{cell} is the number of cells in the x-direction.

The results of convergence studies are shown in Fig. 2. Here, we do not intend to verify 4th-order convergence, which has already been demonstrated in Sec. III(a), but rather attempt to elucidate the practical advantage of using a 4th-order method compared to a 2nd-order method. That is, much faster convergence of the 4th-order simulations is readily seen in Fig. 2. We also compare the simulation results with the analytical predictions obtained from Eq. (36) by neglecting the term $L_n^{-1}\partial/\partial x$ in the left-hand-side of Eq. (36). Such approximation can introduce errors of order $k_\perp L \approx 0.016$, which explains the small difference between the converged simulation results and the analytical predictions observed in Fig. 2.

IV. Conclusions

A numerical instability is found for a high-order finite-volume discretization of magnetized plasma equations governing the dynamics of drift waves. Written in the conservative form such equations contain the advection term $c\boldsymbol{\nabla}\cdot(B^{-1}[\mathbf{b}\times\boldsymbol{\nabla}\phi])$, which can potentially drive fast numerical instability if the identity $\boldsymbol{\nabla}\cdot([\mathbf{b}\times\boldsymbol{\nabla}\phi])\equiv 0$ is not discretely enforced.

The numerical instability is demonstrated for the case of a central-difference fourth-order finite-volume discretization applied to a simple problem of stable drift-waves oscillations with cold ion and adiabatic electron responses. In the absence of the ion polarization term, the growth rate is found to be inversely proportional to the squared grid spacing, $\gamma\sim D_B h^{-2}$, whereas retaining the ion polarization term can bound the growth rate at the level of $\gamma\sim D_B\rho_s^{-2}$. Note that the normalization factor $D_B = cT_e/eB$ corresponds to the Bohm-diffusion scale.

A method to discretely enforce $\boldsymbol{\nabla}\cdot([\mathbf{b}\times\boldsymbol{\nabla}\phi])\equiv 0$ and thus stabilize a numerical scheme is proposed for an arbitrary high-order finite-volume discretization. As a practical example, the method is implemented in the 4th-order finite-volume code COGENT, and demonstrated to work in numerical simulations of stable drift-wave oscillations with adiabatic electrons and the collisionless (universal) drift-wave instability driven by electron kinetic effects.

It is instructive to note that although the condition $\boldsymbol{\nabla}\cdot([\mathbf{b}\times\boldsymbol{\nabla}\phi])\equiv 0$ is consistent with a zero divergence of the advection velocity for the simple case of the fluid description and uniform magnetic field in Eq. (1)-(2), enforcing a discrete zero divergence of an advection velocity in a more general case of a gyrokinetic description, e.g., the 4D gyro-kinetic velocity in Eqs. (25)-(28), does not necessarily eliminate the numerical instability considered in this work. For instance, a high-order finite-volume discretization scheme that provides a discrete zero divergence of a 4D gyro-kinetic velocity regardless of whether the condition $\boldsymbol{\nabla}\cdot([\mathbf{b}\times\boldsymbol{\nabla}\phi])\equiv 0$ is discretely enforced or not is reported in [12] for the case of a nonuniform magnetic field. However, consistent with the analysis presented in this work, numerically stable high-order simulations of drift waves with that discretization are only possible when $\boldsymbol{\nabla}\cdot([\mathbf{b}\times\boldsymbol{\nabla}\phi])\equiv 0$ is discretely enforced.

Finally, it is interesting to point out that the analysis performed in Sec. II for the fluid description of drift waves in a magnetized plasma is of importance to the field of neutral fluid dynamics. In particular, Eqs. (1)-(2) coupled with Eq. (21) represent the linearized version of the Charney-Hasegawa-Mima equation describing drift waves in plasmas [16] as well as the Rossby waves in the atmosphere and oceans of planets [17]. Moreover, considering the conservative form of the standard equations [18] for an incompressible 2D (v_x, v_y) flow written in terms of the vorticity $\bar{\omega} = [\boldsymbol{\nabla}\times\boldsymbol{v}]\cdot\boldsymbol{e}^z$ and the stream function $\bar{\phi}$ [c.f. Eqs. (1)-(2) and (3) or (21)],

$$\frac{\partial\bar{\omega}}{\partial t} + \boldsymbol{\nabla}\cdot([\boldsymbol{\nabla}\bar{\phi}\times\boldsymbol{e}^z]\bar{\omega}) = 0, \tag{38}$$

$$\Delta\bar{\phi} = -\bar{\omega}, \tag{39}$$

and performing the linearization $\bar{\phi} = \bar{\phi}_0 + \delta\bar{\phi}$ around an equilibrium solution $\bar{\phi}_0$, we obtain

$$\frac{\partial}{\partial t}\Delta(\delta\bar{\phi}) + \boldsymbol{\nabla}\cdot\left([\boldsymbol{\nabla}\bar{\phi}_0 \times \boldsymbol{e}^z]\Delta(\delta\bar{\phi})\right) + \boldsymbol{\nabla}\cdot\left([\boldsymbol{\nabla}\delta\bar{\phi} \times \boldsymbol{e}^z]\Delta\bar{\phi}_0\right) = 0, \tag{40}$$

where the second and the third terms contain the terms $\Delta(\delta\bar{\phi})\boldsymbol{\nabla}\cdot([\boldsymbol{\nabla}\bar{\phi}_0 \times \boldsymbol{e}^z]) \equiv 0$ and $\Delta\bar{\phi}_0\boldsymbol{\nabla}\cdot([\boldsymbol{\nabla}\delta\bar{\phi} \times \boldsymbol{e}^z]) \equiv 0$, respectively, which can lead to the numerical instability considered in this work.

Acknowledgments

We would like to thank the reviewer for pointing out the similarity between the model fluid drift-wave equations considered in our work and those describing dynamics of a wide class of neutral fluid systems. This research was supported by the U.S. DOE, Office of Science, Fusion Energy Sciences under Contract DE-AC52-07NA27344.

References

[1] B. B. Kadomtsev and O. P. Pogutse, in *Reviews of Plasma Physics*, edited by M. A. Leontovich (Consultants Bureau, New York, 1965), Vol. 5.

[2] R. J Goldston and P. H. Rutherford "*Introduction to plasma physics*" Taylor & Francis 1995. Print ISBN: 978-0-7503-0183-1.

[3] M. Vinokur, An analysis of finite-difference and finite-volume formulations of conservation laws, J. Comput. Phys. 81 (1989) 1–52.

[4] D.A. Calhoun, C. Helzel, R.J. Leveque, Logically rectangular grids and finite volume methods for PDEs in circular and spherical domains, SIAM Rev. 50 (4) (2008) 723–752.

[5] J. Loffeld and J.A.F. Hittinger, On the arithmetic intensity of high-order finite-volume discretizations for hyperbolic systems of conservation, Int. J. High Perform. Comput. Appl. (2017) 1-28.

[6] P. Colella, M.R. Dorr, J.A.F. Hittinger, and D.F. Martin, High-order, finite-volume methods in mapped coordinates, J. Comput. Phys. 230 (2011) 2952-2976.

[7] P. McCorquodale, M.R. Dorr, J.A.F. Hittinger, P. Colella, High-order finite-volume methods for hyperbolic conservation laws on mapped multiblock grids, *J. Comput. Phys.,* 2015, 288:181-195.

[8] M. R. Dorr, R. H. Cohen, P. Colella, M. A. Dorf, J. A. F. Hittinger, and D. F. Martin, Numerical simulation of phase space advection in gyrokinetic models of fusion plasmas, in Proceedings of the 2010 Scientific Discovery through Advanced Computing (SciDAC) Conference, pages 42–52, Chattanooga, Tennessee, 2010. Oak Ridge National Laboratory. http://computing.ornl.gov/workshops/scidac2010/

[9] M. A. Dorf, R. H. Cohen, M. Dorr, T. Rognlien, J. Hittinger, J. Compton, P. Colella, D. Martin,

and P. McCorquodale, Simulation of neoclassical transport with the continuum gyrokinetic code COGENT, Phys. Plasmas 20 (2013) 012513.

[10] M. A. Dorf, R. H. Cohen, M. Dorr, T. Rognlien, J. Hittinger, J. Compton, P. Colella, D. Martin, and P. McCorquodale, Numerical modelling of geodesic acoustic mode relaxation in a tokamak edge, Nucl. Fusion 53 (2013) 063015.

[11] M. A. Dorf, M. R. Dorr, J. A. Hittinger, R. H. Cohen, and T. D. Rognlien, Continuum kinetic modeling of the tokamak plasma edge, Phys. Plasmas 23 (2016) 056102.

[12] M. Dorr, J. Hittinger, M. Dorf, P. Colella, P. Shwartz, and D. Ghosh, High-order discretization of a gyrokinetic Vlasov model in edge plasma geometry, submitted to J. Comp. Phys. (2018).

[13] Mathematica is a software product of Wolfram Research, Champaign, Illinois, 61820.

[14] T. S. Hahm, Nonlinear gyrokinetic equations for turbulence in core transport barriers, Phys. Plasmas 3 (1996) 4658-4664

[15] J. W. Banks and J. A. F. Hittinger, A New Class of Nonlinear Finite-Volume Methods for Vlasov Simulation, IEEE Transactions on Plasma Science 38(9) (2010) 2198-2207.

[16] A. Hasegawa, K. Mima, Pseudo-three-dimensional turbulence in magnetized nonuniform plasma, Phys. Fluids 21 (1978) 87–92.

[17] J.G. Charney, On the scale of atmospheric motions, Geophys. Publ. Oslo 17 (1948) 1–17.

[18] L.D. Landau, E.M. Lifshift Fluid Mechanics, Pergamon, Oxford (1959).